Annals of Pharmacy Practice and Pharmacotherapy
ISSN: 3062-4436
2021, Volume 1, Page No: 182-200

Available online at: www.galaxypub.co/page/journals

Galaxy Publication

SNX10 Promotes Chaperone-Mediated Autophagic Degradation of DEPDC5 in Normal Intestinal Epithelial Cells: Reversal by α-Hederin

Lucas Moreau[1]*, Camille D. Bernard[2]

[1]Department of Clinical Pharmacy, Faculty of Pharmacy, University of Paris-Saclay, Paris, France.
[2]Department of Pharmacotherapy, Faculty of Pharmacy, University of Geneva, Geneva, Switzerland.

***E-mail** ✉ l.moreau.pharma@outlook.com

Received: 06 September 2021; **Revised:** 06 December 2021; **Accepted:** 08 December 2021

ABSTRACT

Colorectal carcinoma (CRC) arises from genetic alterations in healthy intestinal epithelial cells (IECs). Sorting nexin 10 (SNX10) functions as a suppressor of CRC progression and modulates chaperone-mediated autophagy (CMA), a process linked to CRC development and glycolytic metabolism. DEP domain-containing protein 5 (DEPDC5) serves as an inhibitory regulator upstream of mTOR complex 1 (mTORC1). The compound α-hederin displays antitumor activity against CRC. Earlier work from our group showed that reducing SNX10 levels in normal human IECs enhanced glycolytic flux while lowering DEPDC5 levels, effects that α-hederin counteracted. The precise underlying pathway, however, remained unclear. In the present investigation, we sought to clarify how SNX10 controls DEPDC5 stability and the role of α-hederin therein. Results revealed that SNX10 reduction hastened DEPDC5 proteolysis, leading to mTORC1 hyperactivation dependent on increased CMA activity and improved lysosomal performance. SNX10 directly associated with DEPDC5, directing it toward lysosomal compartments for breakdown, thereby elevating mTORC1-driven glycolysis. Re-expression of SNX10 in knockdown cells abolished these alterations. Furthermore, α-hederin engaged the SNX10–DEPDC5 assembly, weakening their interaction and blocking CMA-directed DEPDC5 proteolysis. This action suppressed excessive mTORC1 signaling and ultimately normalized the heightened glycolysis triggered by SNX10 loss. Collectively, our findings establish, for the first time, that SNX10-orchestrated DEPDC5 proteolysis represents a critical pathway in the oncogenic conversion of normal IECs, a process modulated by α-hederin.

Keywords: α-hederin, IECs, SNX10, DEPDC5, Chaperone-mediated autophagy, Lysosome

How to Cite This Article: Moreau L, Bernard CD. SNX10 Promotes Chaperone-Mediated Autophagic Degradation of DEPDC5 in Normal Intestinal Epithelial Cells: Reversal by α-Hederin. Ann Pharm Pract Pharmacother. 2021;1:182-200. https://doi.org/10.51847/r4zodtw5UE

Introduction

Colorectal cancer (CRC) ranks among the most severe malignancies globally, holding the third position in incidence and the second in cancer-related deaths [1]. The complete mechanisms driving CRC onset are still incompletely understood. Alterations such as mutations, loss of genetic material, and dysregulated gene expression in intestinal epithelial cells (IECs) constitute the primary triggers of colorectal tumorigenesis [2]. Consequently, exploring gene roles in non-malignant IECs holds promise for uncovering preventive therapeutic targets against CRC.

Sorting nexin 10 (SNX10) exerts tumor-suppressive effects in CRC [3, 4] and participates in controlling endosomal-lysosomal trafficking [5, 6], a system essential for the execution of chaperone-mediated autophagy (CMA). CMA represents a targeted autophagic pathway that maintains cellular equilibrium through chaperone-guided lysosomal proteolysis [7] and is frequently elevated in cancers to support oncogenic growth and survival [8]. Prior reports documented CMA upregulation in SNX10-deficient HCT116 CRC cells, fostering cell expansion and resistance to stress [3]. Similar activation occurred in SNX10-null mice via stabilization of lysosome-associated membrane protein 2A (LAMP-2A), subsequent AMPK pathway engagement, and mitigation of alcohol-related liver damage and fat accumulation [9]. In murine hepatocytes with reduced SNX10, CMA

induction arose from blocked cathepsin A (CTSA) maturation—a protease critical for LAMP-2A turnover—ultimately alleviating hepatic lipid buildup [10]. Enhanced glycolysis, the predominant energy pathway in malignant cells, is markedly intensified across numerous cancers relative to healthy tissues and drives tumor advancement [11]. Multiple investigations confirmed that heightened CMA boosts glycolytic rates in malignancies, including breast carcinoma [12] and colorectal tumors [13]. As terminal degradative structures in CMA, lysosomes function as central nodes for metabolic signaling [14], influencing mTORC1 [15] and AMPK [16] cascades. Our prior research indicated that SNX10 governs glucose utilization in human IECs [17]. The manner in which it affects lysosomal operations, however, is undetermined, as is potential interplay between SNX10-linked CMA and glycolytic regulation.

The mTORC1 complex orchestrates cellular growth and metabolic responses to environmental cues while preserving internal balance. Activated at lysosomal surfaces, it phosphorylates effectors like p70S6K and 4EBP1 to stimulate biosynthetic processes [16]. DEPDC5 inhibits mTORC1 activity and has emerged as a suppressor in gastrointestinal stromal tumors by restricting mesenchymal proliferation [18]. Recent evidence showed diminished DEPDC5 in CRC patient tumors, associating with poorer survival outcomes [19]. Regulatory pathways governing DEPDC5 during carcinogenesis, nevertheless, are largely unexplored.

α-Hederin, a pentacyclic triterpene saponin derived from Fructus Akebia, acts as a novel inhibitor of autophagy by obstructing terminal flux [20]. It also curbs lung carcinoma expansion through suppression of SIRT6-reliant glycolysis [21] and triggers autophagic cell death in CRC lines via AMPK/mTOR modulation [22]. Our earlier work revealed that α-hederin impedes terminal autophagic stages, causing substantial vesicle buildup and proteostatic imbalance in human CRC models [23]. Together, these observations highlight α-hederin's influence on autophagic and glycolytic pathways. We previously observed that α-hederin normalized the excessive glycolysis and restored DEPDC5 protein levels diminished by SNX10 silencing in IECs [17], yet the detailed mechanism was undefined. The current work was designed to bridge this knowledge gap and delineate the molecular basis involved.

Materials and Methods

Compounds and reagents

High-purity α-hederin (>98%) was obtained from Chengdu Herbpurify Co., Ltd. (Chengdu, China) and solubilized in DMSO to the required concentrations. The proteasome inhibitor MG-132 (ab141003) and the vacuolar ATPase inhibitor bafilomycin A1 (ab120497) were acquired from Abcam (Cambridge, UK). Additional inhibitors, including rapamycin (HY-10219), cycloheximide (HY-12320), chloroquine (HY-17589A), and Pronase E (HY-114158), were purchased from MedChemExpress (Monmouth Junction, NJ, USA). A range of antibodies was used: those recognizing mTOR (ab2732), Raptor (ab40768), p70S6K (ab32529), 4EBP1 (ab32024), phosphorylated 4EBP1 (ab278686), LAMP-2A (ab125068 and ab18528), along with fluorescent secondary antibodies Alexa Fluor® 594 goat anti-rabbit (ab150080), Alexa Fluor® 647 goat anti-mouse (ab150115), Alexa Fluor® 488 goat anti-mouse (ab150113), and Alexa Fluor® 488 goat anti-rabbit (ab150077) were all from Abcam. Phosphorylated mTOR (5536S), GβL (3274S), c-Myc (5605T), LDHA (3582T), PKM2 (4053T), HRP-conjugated anti-mouse (7076P2), and anti-rabbit (7074P2) secondaries were sourced from Cell Signaling Technology (Danvers, MA, USA). The SNX10-specific antibody (sc-293380) was from Santa Cruz Biotechnology (Dallas, TX, USA). Antibodies for β-Tubulin (M20005), DEPDC5 (TA7028), and phosphorylated DEPDC5 (Ser1002) (TA8614) were supplied by Abmart (Shanghai, China). Further antibodies targeting mTOR (66888-1-Ig), HSC70 (ab51052), LAMP2 (66301-1-Ig), and Flag tag (66008-4-Ig) were provided by Proteintech (Wuhan, China).

Maintenance of cell lines

Human colorectal carcinoma lines (DLD-1, LoVo, Caco-2, SW620, HT29) and normal intestinal epithelial lines (FHC, NCM460), together with HEK-293T cells, were all procured from ATCC (Rockville, Maryland, USA). Cultures were grown in appropriate basal media—RPMI-1640, Ham's F-12K, DMEM, Leibovitz's L-15, or McCoy's 5A—each supplemented with 10% fetal bovine serum and 1% penicillin-streptomycin mixture, and incubated at 37°C under 5% CO_2 in a humidified incubator.

Protein immunoblotting

Harvested cells were disrupted in chilled lysis buffer (P0013J; Beyotime, Shanghai, China) fortified with complete protease and phosphatase inhibitor cocktails (11836153001 and 4906845001; Roche, Basel, Switzerland). Protein yields were measured via BCA assay (23225; Thermo Scientific, Waltham, MA, USA). Samples containing 20 μg protein were fractionated by SDS-PAGE, transferred to PVDF membranes, and blocked for 2 h in 5% skim milk dissolved in PBST at ambient temperature. Primary antibody probing occurred overnight at 4°C, followed by secondary antibody incubation for 1 h at room temperature. Chemiluminescent signals were captured using ECL reagent (32209; Thermo Scientific) on a Bio-Rad ChemiDoc XRS+ imager (Hercules, CA, USA).

Total RNA preparation and quantitative RT-PCR

RNA was isolated from cultured cells with TRIzol reagent (15596018; Invitrogen, Carlsbad, CA, USA) per the supplied protocol. Purity and concentration were evaluated on a NanoDrop 1000 instrument (Thermo Fisher Scientific). First-strand cDNA was generated from 1 μg RNA using the Evo M-MLV reverse transcription kit with genomic DNA remover (AG11728; Accurate Biotechnology, Changsha, China). Amplification was performed with SYBR Green-based master mix (AG11701; Accurate Biotechnology) on an Applied Biosystems StepOnePlus platform (Foster City, CA, USA). Fold changes in transcript abundance were computed relative to β-actin housekeeping control by the $2^{-\Delta\Delta Ct}$ approach.

Construction of lentiviral vectors and stable transduction

Helper plasmids pMD2.G (P0262) and psPAX2 (P0261), plus the shRNA expression backbone pLVshRNA-EGFP(2A)Puro (P0684), were acquired from Miao Ling Biotech (Wuhan, China). Double-stranded oligonucleotides were ligated into EcoRI/BamHI-restricted vector (enzymes JE201-01 and JB101-01; TransGen, Beijing, China). Recombinant shSNX10 or control vectors were introduced with packaging plasmids into near-confluent HEK-293T cells. Viral particles were recovered from culture media at 48 and 72 h, filtered (0.45 μm), and applied to target FHC or NCM460 cells in the presence of 10 μg/mL polybrene (P8001350; YEASEN, Shanghai, China) using a 1:1 virus-to-basal medium ratio for 24 h. Puromycin selection (2 μg/mL; ST551; Beyotime) established stable pools, with knockdown validated by RT-qPCR and immunoblotting.

Plasmid delivery by transient transfection

Specified expression constructs were delivered using Lipo8000 reagent (C0533; Beyotime). DNA and transfection reagent were separately diluted in Opti-MEM without serum (31985070; Invitrogen), combined, and incubated 25 min under standard culture conditions to form complexes. These were added to HEK-293T, FHC, or NCM460 cultures at 60–70% confluence (fresh medium added 2 h beforehand). Efficacy was confirmed through qPCR and protein analysis.

Immunoprecipitation experiments

Cells were solubilized in ice-cold buffer containing protease inhibitors for 30 min, then cleared by centrifugation (12, 000 rpm, 15 min). Quantified lysates were rotated overnight at 4°C with appropriate primary antibodies coupled to protein A+G magnetic beads (P2179; Beyotime). Captured immune complexes underwent three washes in lysis buffer before elution and resolution by SDS-PAGE followed by immunoblot detection.

Immunofluorescence analysis

Cells were plated at a density of 2.5 × 10^4 cells per well on glass coverslips in 24-well plates and subjected to the specified treatments. Following exposure to compounds, cells underwent three rinses with ice-cold phosphate buffered saline (PBS), fixation with 4% paraformaldehyde for 10 min, and permeabilization using Saponin (P0095; Beyotime) for 30 min at room temperature (RT). After blocking with 5% BSA in PBS for 1 h at RT, samples were incubated overnight at 4 °C with primary antibodies. On the following day, cells were washed three times in PBST and then exposed to Alexa Fluor®-conjugated secondary antibodies for 2.5 h at RT. Nuclear counterstaining was achieved using antifade mounting medium containing 2-(4-Amidinophenyl)-6-indolecarbamidine dihydrochloride (DAPI) (P0131; Beyotime) for 10 min. Fluorescence images were acquired with either an inverted fluorescent microscope (THUNDER Imaging Systems CN, Leica, Wetzlar, Germany) or a confocal laser-scanning microscope (Leica).

Lysosomal fractionation

Lysosomes were purified from cultured cells via differential centrifugation of a light mitochondrial-lysosomal pellet through a discontinuous metrizamide gradient, employing a modified rapid lysosome isolation kit (LY-034; Invent Biotechnologies, Eden Prairie, MN, USA) in accordance with the manufacturer's guidelines. The final purified lysosomal fraction was resuspended in radio immunoprecipitation assay (RIPA) buffer prior to downstream immunoblot analysis.

Live-cell lysosomal labeling

LysoTracker Red (C1046; Beyotime), a red-fluorescent probe that selectively accumulates in acidic compartments, was utilized to label lysosomes in living cells and assess intralysosomal pH. Cells were grown in 6 cm dishes until reaching 70%–80% confluence, then exposed to α-hederin, chloroquine (CQ), or Earle's balanced salt solution (EBSS) (C0214; Beyotime) — or left untreated — for 24 h. Subsequently, cells were incubated with 50 nM LysoTracker Red for 1 h at 37 °C in the dark. After PBS washing, nuclei were counterstained with Hoechst 33342 (C1022; Beyotime) for 10 min at RT. Fluorescence images were obtained using an inverted fluorescence microscope (Nikon Eclipse Ti, Nikon, Tokyo, Japan).

For quantitative assessment of LysoTracker uptake in live cells, excess dye was removed by two PBS washes, cells were detached using EDTA-free trypsin, rinsed again with PBS, and lysosomal content was quantified by flow cytometry (Beckman Coulter, Brea, CA, USA) with excitation at 577 nm.

Cell proliferation evaluation

In the cell viability assay, cells were seeded at 2 × 10^3 cells/well in 96-well plates. After 1, 2, 3, 4, and 5 days of culture, 10% Cell Counting Kit-8 (CCK-8) (C0037; Beyotime) was added to each well, and absorbance was recorded at 450 nm on a microplate reader (TECAN SPARK 10 M, TECAN, Männedorf, Switzerland).

For colony formation assays, single-cell suspensions were plated at approximately 800 cells/well in 6-well plates and cultured for 2 weeks. Colonies were fixed with 4% paraformaldehyde for 10 min, stained with 0.1% crystal violet for 30 min, and then enumerated.

In the EdU incorporation assay, 2.5 × 10^4 cells/well were seeded in 24-well plates, and EdU-labeled proliferating cells were detected and imaged using an inverted fluorescence microscope (Nikon Eclipse Ti, Nikon).

Glycolytic enzyme activity measurement

Activities of critical glycolytic enzymes, namely lactate dehydrogenase (LDH) (BC0685) and pyruvate kinase (PK) (BC0545), were measured following the protocols provided in commercial assay kits from Beijing Solarbio Science & Technology Co., Ltd. (Beijing, China).

Cytotoxicity screening

To determine suitable drug doses, cells were plated at 8 × 10^3 cells/well in 96-well plates and exposed to varying drug concentrations for 24 h. Cell cytotoxicity was evaluated using the 3-(4, 5-dimethylthiazol-2-yl)-2, 5-diphenyl tetrazolium bromide (MTT) assay as per the manufacturer's instructions (C0009S; Beyotime).

In silico molecular docking

The three-dimensional structure of SNX10 was retrieved from the Protein Data Bank (PDB ID: 4PZG), and that of DEPDC5 from the Protein Data Bank (PDB ID: 6CET). The two-dimensional structure of α-hederin was obtained from PubChem (PubChem CID: 73296). SNX10 and DEPDC5 were designated as receptor proteins, while α-hederin served as the ligand. Potential protein–protein interactions were predicted via the ZDOCK server. Docking simulations were conducted with AutoDock 2, involving initial coarse docking by a simulated annealing approach followed by refinement through a genetic algorithm.

Cellular thermal shift assay (CETSA)

Cells grown in 100-mm dishes until reaching 80% confluence were exposed to DMSO or α-hederin for 6 h. Following trypsin detachment, cells were resuspended in PBS containing protease and phosphatase inhibitors, then split into eight equal portions in 200 μL PCR tubes. Each aliquot was subjected to heating at 49, 52, 55, 58, 61, 64, 67, and 70 °C for 5 min using a thermal cycler (Bio-Rad). Soluble proteins were isolated through three rounds of freeze–thaw cycles in liquid nitrogen, followed by centrifugation at 12, 000 rpm for 10 min. The resulting supernatants were subjected to Western blot analysis using antibodies targeting SNX10 or DEPDC5.

Drug affinity responsive target stability (DARTS)

Cells were collected and lysed in RIPA buffer supplemented with protease and phosphatase inhibitors. Equal volumes of lysate were distributed into five Eppendorf tubes. Samples were then incubated with 0.1% DMSO or different concentrations of α-hederin for 1 h at room temperature under gentle agitation. Pronase E (25 μg/mL) was added for proteolytic digestion lasting 30 min. Reactions were terminated by adding SDS-PAGE loading buffer, and target proteins were detected via Western blotting with antibodies against SNX10 or DEPDC5.

Statistical evaluation

All data were processed and expressed as mean ± standard deviation (SD) using GraphPad Prism 9.0. Comparisons between two groups were performed with Student's t-test, while multiple groups were analyzed via one- or two-way analysis of variance (ANOVA) followed by Bonferroni's post-hoc test. Each experiment was repeated independently at least three times with biological replicates. A value of $P < 0.05$ was regarded as statistically significant.

Results and Discussion

Depletion of SNX10 promoted lysosomal-mediated degradation of DEPDC5 in FHC and NCM460 cells

In prior work [17], three distinct shRNAs targeting the SNX10 gene were developed to silence SNX10 expression in FHC and NCM460 cells, generating stable knockdown lines designated shSNX10-1 (sh1), shSNX10-2 (sh2), and shSNX10-3 (sh3). The lines exhibiting maximal knockdown efficiency—sh1 for FHC and sh2 for NCM460—were chosen for further experiments. Unexpectedly, DEPDC5 protein levels were markedly lower in SNX10-depleted normal human intestinal epithelial cells (IECs). This led us to propose that SNX10 exerts positive control over DEPDC5 stability. Although the human DEPDC5 gene (Gene ID: 9681; Mass: 181.264 kDa) produces 13 transcripts and 8 protein isoforms of varying sizes, integration of data from sources including NCBI, MANE, RefSeq Select, Ensembl, and UniProt consistently identified the transcript NM_001242896.3 as the primary, canonical, clinically relevant, highly conserved, most abundant, and longest variant. Primers specific to this transcript were designed to assess DEPDC5 expression in SNX10-knockdown IECs. Results revealed a substantial reduction in DEPDC5 protein, but no alteration in mRNA levels, in shSNX10 cells **(Figures 1a and 1b)**. To explore SNX10's role further, a pCR3.1-hSNX10 plasmid carrying an mCherry tag was constructed for overexpression and rescue studies in shSNX10 lines; successful overexpression was verified by qPCR and immunoblotting. Re-expression of SNX10 partially restored DEPDC5 protein abundance without affecting its mRNA, indicating post-transcriptional regulation by SNX10.

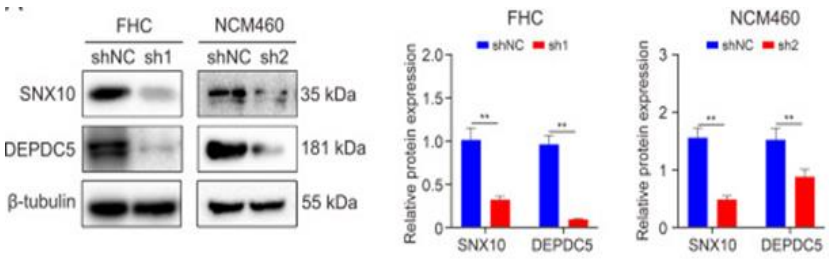

a)

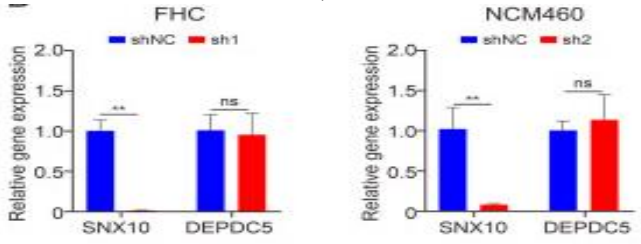

b)

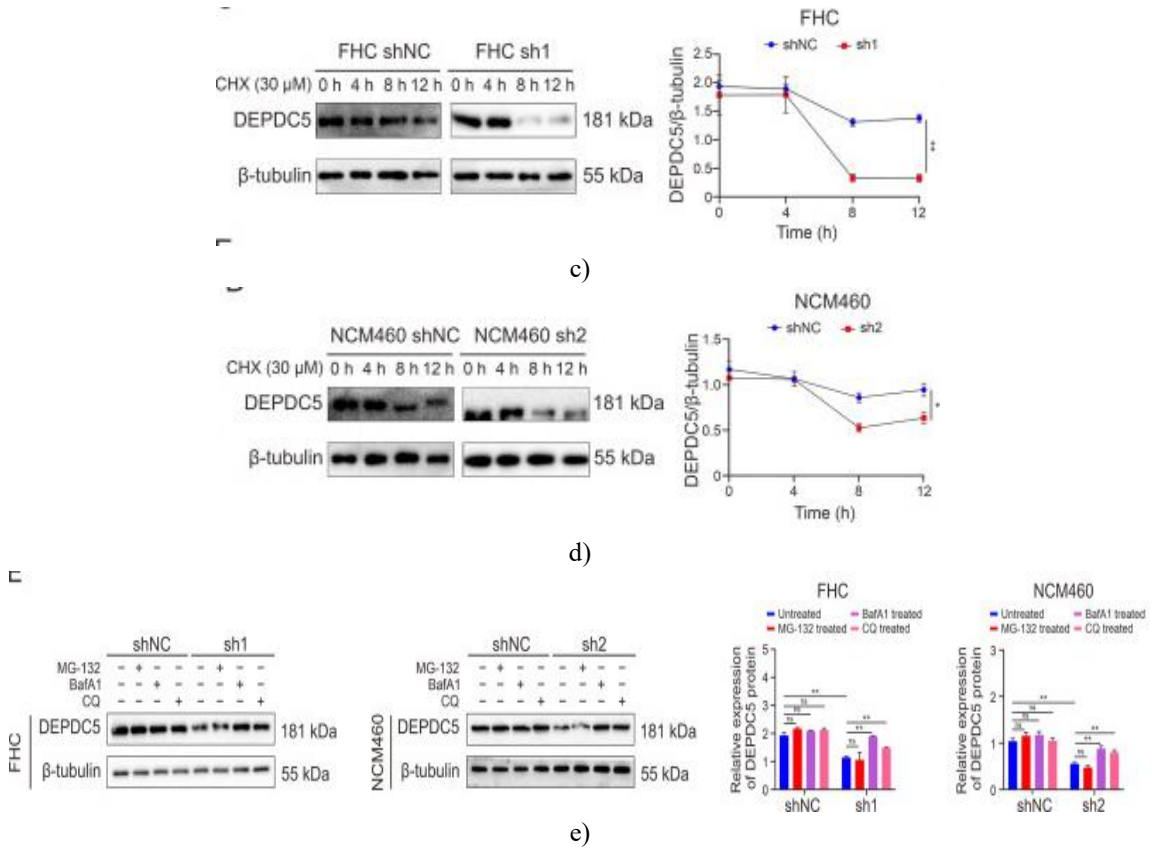

Figure 1. Sorting nexin 10 (SNX10) depletion enhanced DEP domain-containing 5 (DEPDC5) protein turnover in FHC and NCM460 cells. (a) Western blot assessment of SNX10 and DEPDC5 protein in shNC and shSNX10 lines. (b) qPCR measurement of SNX10 and DEPDC5 mRNA in shNC and shSNX10 cells. (c, d) Time-course analysis of DEPDC5 stability by Western blotting in FHC shNC and shSNX10-1 (sh1) cells (c) and NCM460 shNC and shSNX10-2 (sh2) cells (d) following treatment with cycloheximide (CHX; 30 μM) for 0, 4, 8, and 12 h. (e) Immunoblot detection of DEPDC5 in shNC and shSNX10 cells after 24 h exposure to MG-132 (10 μM), bafilomycin A1 (BafA1; 100 nM), or chloroquine (CQ; 20 μM). Values represent means ± SD. ∗P < 0.05, ∗∗P < 0.01 compared to control; ns: not significant.

Reduced DEPDC5 protein could stem from impaired synthesis, accelerated degradation, or both. To test this, protein translation was blocked with cycloheximide (CHX), and DEPDC5 half-life was monitored via CHX chase. In both cell types, DEPDC5 levels declined over time post-CHX, with a notably shorter half-life in shSNX10 compared to shNC cells **(Figures 1c and 1d)**. Thus, SNX10 loss destabilizes DEPDC5 by enhancing its post-translational breakdown.

To identify the degradation route, inhibitors targeting the two primary eukaryotic systems—proteasome and lysosome—were employed. shNC and shSNX10 cells were treated with the proteasomal blocker MG-132 (10 μM), or lysosomal inhibitors bafilomycin A1 (100 nM) and CQ (20 μM). In shNC cells, none of these agents altered DEPDC5 levels significantly. In contrast, lysosomal inhibitors (but not MG-132) prevented the DEPDC5 reduction in shSNX10 lines **(Figure 1e)**. These findings demonstrate that SNX10 controls DEPDC5 stability specifically via the lysosomal degradation pathway.

DEPDC5 served as a chaperone-mediated autophagy (CMA) substrate, forming a complex with SNX10 that facilitated its recruitment to lysosomes for CMA-dependent degradation

SNX10 is known to critically modulate CMA function [3, 9, 10]. Every CMA substrate harbors KFERQ-like pentapeptide motifs essential for recognition and degradation through this pathway [7]. These motifs enable binding to molecular chaperones: heat shock cognate protein 70 (HSC70) identifies the motif in target proteins, while lysosome-associated membrane protein type 2A (LAMP-2A) on the lysosomal membrane mediates substrate translocation into the lysosomal lumen for breakdown. To determine whether DEPDC5 possesses such motifs, we aligned its amino acid sequences across multiple species (10 representative species shown). The

analysis revealed two conserved canonical CMA motifs (QKVEF and VRLEQ) **(Figure 2a)**, indicating that DEPDC5 qualifies as a potential CMA substrate and that SNX10 depletion may enhance its degradation via a CMA-reliant mechanism.

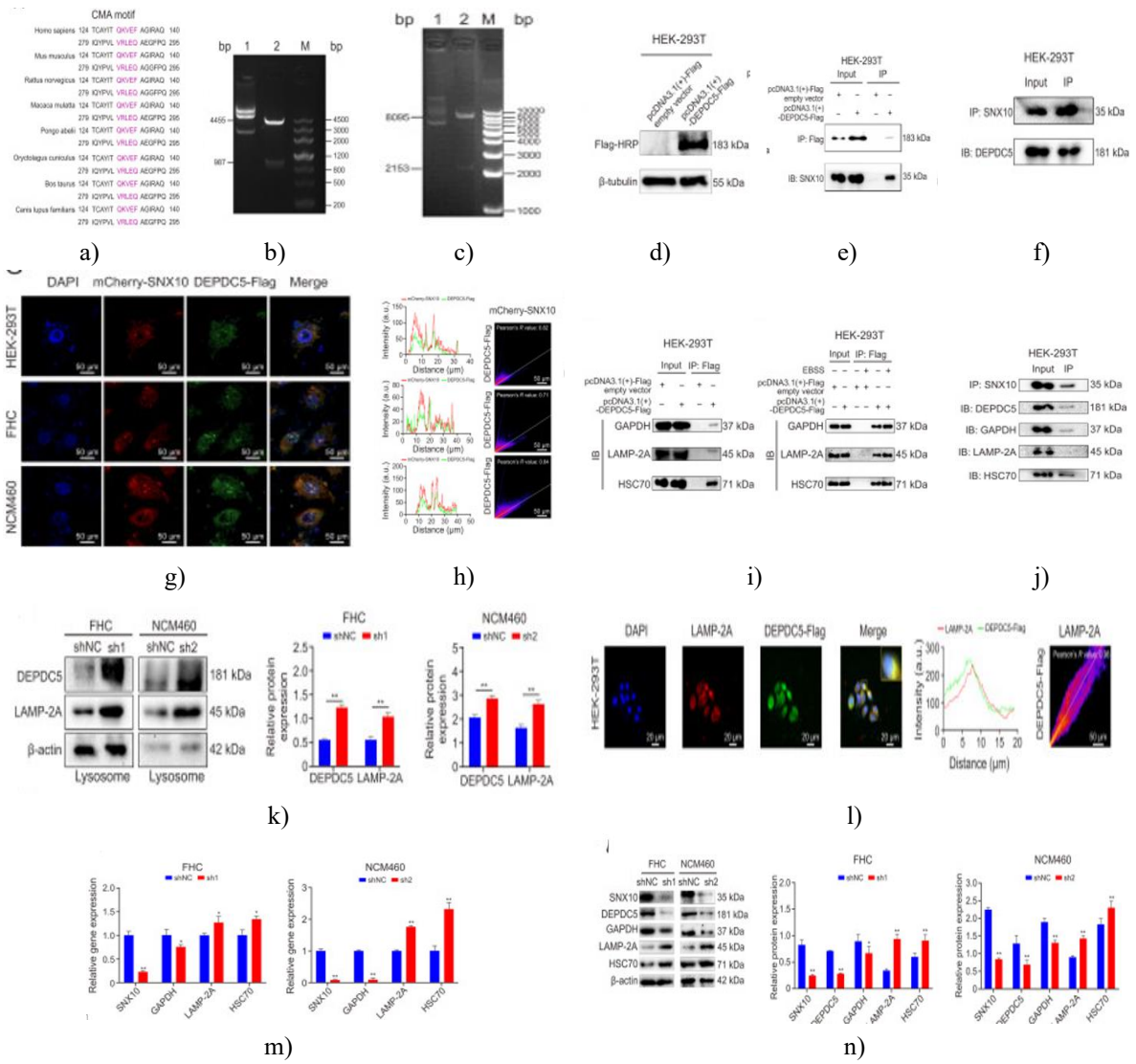

Figure 2. Depletion of sorting nexin 10 (SNX10) enhanced DEP domain-containing 5 (DEPDC5) turnover through the chaperone-mediated autophagy (CMA) pathway. (a) Multi-species alignment of DEPDC5 sequences; conserved CMA motifs highlighted in pink. (b) Double restriction digestion verification of pcDNA3.1(+)-Flag plasmid. bp: base pair; 1: undigested pcDNA3.1(+)-Flag; 2: BglII-XhoI fragments (expected sizes: 987/4455 bp); M: DNA marker. (c) Single restriction digestion of pcDNA3.1(+)-DEPDC5-Flag plasmid. bp: base pair; 1: undigested pcDNA3.1(+)-DEPDC5-Flag; 2: EcoRI fragments (expected sizes: 2153/8095 bp); M: DNA marker. (d) Western blot confirmation of Flag-tagged DEPDC5 expression from the recombinant plasmid. (e, f) Co-immunoprecipitation (Co-IP) validation of DEPDC5-SNX10 interaction using anti-Flag (e) and anti-SNX10 (F) antibodies. (g) Confocal imaging of DEPDC5 and SNX10 co-localization, with qualitative/quantitative assessment via ImageJ. (h) Co-IP of DEPDC5 with core CMA pathway components. (i) Co-IP of DEPDC5 with CMA components under Earle's balanced salt solution (EBSS)-stimulated CMA activation. (j) Co-IP of SNX10 with CMA-associated proteins. (k) Lysosomal fractions isolated from shNC and shSNX10 intestinal epithelial cells (IECs) analyzed by Western blotting with indicated antibodies. (l) Confocal imaging of DEPDC5 and LAMP-2A co-localization, with ImageJ-based qualitative/quantitative evaluation. (m, n) qPCR (m) and Western blot (n) assessment of CMA-related gene and protein levels following SNX10 knockdown. Values shown as means ± SD. ∗P < 0.05, ∗∗P < 0.01 versus

shNC. sh1: shSNX10-1; sh2: shSNX10-2; GAPDH: glyceraldehyde-3-phosphate dehydrogenase; LAMP-2A: lysosome-associated membrane protein type 2A; HSC70: heat shock cognate protein 70.

The preceding evidence establishes that SNX10 governs DEPDC5 stability in a lysosome-dependent fashion. We next examined whether SNX10 actively recruits DEPDC5 to lysosomes. To test this and elucidate interactions between DEPDC5, SNX10, and CMA components, we employed the empty vector pcDNA3.1(+)-Flag and a Flag-tagged full-length DEPDC5 construct based on the canonical MANE Select transcript (Gene ID: 9681; NM_001242896.3; longest isoform; molecular mass: 181.264 kDa) termed pcDNA3.1(+)-DEPDC5-Flag **(Figures 2b and 2c)**. Successful expression was confirmed by transfecting HEK-293T cells, harvesting at 72 h post-transfection, and performing immunoblotting: empty vector samples lacked specific bands, whereas DEPDC5-Flag samples displayed a distinct band at approximately 183 kDa (Flag tag ~2.73 kDa, DEPDC5 ~181 kDa) **(Figure 2d)**, verifying proper plasmid construction and fusion protein production.

Overexpression of DEPDC5-Flag in HEK-293T cells followed by Co-IP with anti-Flag antibody revealed co-precipitation of endogenous SNX10, demonstrating direct physical association **(Figure 2e)**. Reciprocal IP using anti-SNX10 antibody similarly confirmed this interaction **(Figure 2f)**. Confocal microscopy further showed substantial cytoplasmic overlap between DEPDC5 (green) and SNX10 (red), with ImageJ analysis quantifying robust co-localization **(Figure 2g)**. Collectively, these data establish DEPDC5 as a novel interacting partner of SNX10.

Given the presence of two canonical CMA motifs in DEPDC5 **(Figure 2a)**, we probed its association with core CMA machinery. Anti-Flag Co-IP pulled down LAMP-2A, HSC70, and GAPDH (a known CMA substrate), confirming DEPDC5 engagement with these proteins **(Figure 2h)**. This binding intensified under EBSS-induced CMA activation **(Figure 2i)**, solidifying DEPDC5 as a bona fide CMA substrate. Notably, SNX10 sequences across species lack classic CMA motifs. Reciprocal Co-IP with anti-SNX10 antibody failed to detect direct LAMP-2A binding but recovered GAPDH and HSC70 **(Figure 2j)**, suggesting SNX10 does not undergo CMA degradation itself, possibly due to absent motifs or incompatible structure.

To assess lysosomal targeting, purified lysosomal fractions from shNC and shSNX10 IECs were analyzed: baseline DEPDC5 association with lysosomes was observed in shNC cells, while shSNX10 fractions exhibited marked DEPDC5 enrichment alongside elevated LAMP-2A **(Figure 2k)**. Confocal imaging displayed pronounced cytoplasmic co-localization of DEPDC5 (green) with LAMP-2A (red), corroborated by ImageJ quantification **(Figure 2l)**. These findings confirm that DEPDC5 is a CMA substrate that associates with key CMA effectors (e.g., LAMP-2A and HSC70), undergoes lysosomal delivery, and is degraded therein—further substantiating that SNX10 forms a complex with DEPDC5 to shuttle it to lysosomes for CMA-mediated breakdown.

Given that elevated LAMP-2A levels are known to enhance CMA flux and having established DEPDC5 as a new CMA target, we next evaluated CMA flux in shNC and shSNX10 lines from FHC and NCM460 cells. Results indicated lower gene and protein abundance of GAPDH alongside higher levels of HSC70 and LAMP-2A in SNX10-depleted cells **(Figures 2m and 2n)**, pointing to heightened CMA flux in IECs upon SNX10 loss. Furthermore, data from the prior SNX10 rescue study demonstrated that restoring SNX10 expression mitigated DEPDC5 protein loss and normalized CMA marker alterations in knockdown lines. Specifically, SNX10 restoration counteracted the rise in HSC70 and LAMP-2A and the drop in GAPDH triggered by depletion, highlighting SNX10's key role in modulating CMA flux and DEPDC5 stability in normal human IECs. As lysosomal-associated membrane protein-1 (LAMP-1) represents another major lysosomal marker, we assessed its levels and observed no alteration in protein expression following SNX10 knockdown in FHC and NCM460 cells. We then tested whether LAMP-1 contributes to SNX10-dependent DEPDC5 turnover. Data revealed no association between LAMP-1 and DEPDC5, despite its interaction with SNX10, indicating that the CMA-limiting factor LAMP-2A—rather than LAMP-1—mediates SNX10-driven DEPDC5 breakdown, reinforcing DEPDC5 as a CMA target **(Figures 2a, 2h, 2i and 2l)**. This suggests SNX10 functions to suppress CMA, despite lacking direct binding to the CMA-limiting protein LAMP-2A **(Figure 2j)**. Thus, it is plausible that SNX10 modulates CMA flux via direct association with DEPDC5.

Augmented lysosomal activity from SNX10 depletion drove CMA-dependent DEPDC5 turnover

To substantiate the elevated CMA flux in shSNX10 cells **(Figures 2m and 2n)**, we applied EBSS (a CMA inducer) and CQ (an autophagy blocker). Following 24 h EBSS exposure, shSNX10 cells displayed more

pronounced reductions in GAPDH and elevations in LAMP-2A and HSC70 relative to shNC cells, accompanied by intensified CMA flux and marked DEPDC5 protein loss under EBSS stimulation. As anticipated, CQ suppressed lysosomal function and halted DEPDC5 turnover. Notably, when added atop EBSS, CQ elevated LAMP-2A and HSC70 protein while reversing the declines in DEPDC5 and GAPDH in both shNC and shSNX10 lines; inter-group disparities in DEPDC5, GAPDH, LAMP-2A, and HSC70 levels were diminished or abolished **(Figure 3a)**. CMA induction manifests as a shift in GAPDH fluorescence from diffuse to punctate upon substrate delivery to lysosomes, with puncta count serving as a robust CMA metric. Immunofluorescence co-labeling of native GAPDH (yellow) and LAMP-2A (red) revealed diffuse patterns in shNC cells versus punctate distributions in shSNX10 cells, where puncta represented GAPDH and LAMP-2A bound to lysosomal surfaces. Puncta numbers rose substantially, and GAPDH–LAMP-2A overlap intensified markedly, signifying that SNX10 loss boosted lysosomal autophagy and triggered intracellular CMA **(Figure 3b)**. Critically, GAPDH–LAMP-2A overlap was evident. This effect intensified after 24 h EBSS treatment. Adding CQ to EBSS attenuated the pronounced differences in LAMP-2A and GAPDH between shNC and shSNX10 cells. Overall, these data validate upregulated CMA flux in shSNX10 cells, reinforcing SNX10's pivotal involvement in controlling CMA flux [3, 9, 10].

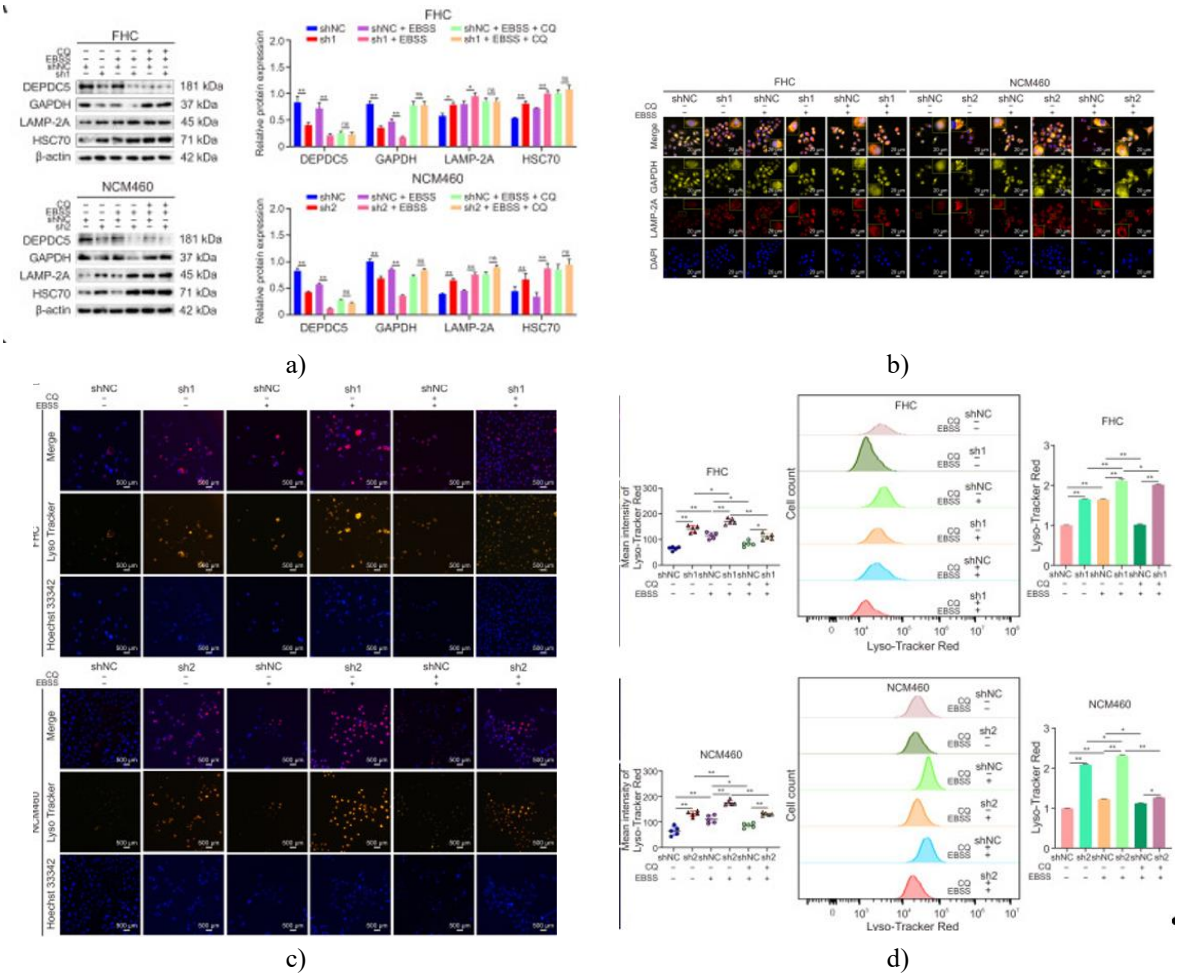

Figure 3. Depletion of sorting nexin 10 (SNX10) elevated lysosomal performance and chaperone-mediated autophagy (CMA) flux. (a) Western blot analysis of DEP domain containing 5 (DEPDC5) and CMA markers in shNC and shSNX10 cells ± chloroquine (CQ) and Earle's balanced salt solution (EBSS) exposure. (b) Co-labeling of native glyceraldehyde-3-phosphate dehydrogenase (GAPDH) (yellow) and lysosome-associated membrane protein type 2A (LAMP-2A) (red) in shNC and shSNX10 cells. (c) Representative Lyso-Tracker Red (50 nM, 1 h) staining images ± CQ and EBSS. (d) Flow cytometric quantification of lysosomal activity via Lyso-Tracker Red (50 nM, 1 h). Values are means ± SD. ∗P < 0.05, ∗∗P < 0.01 versus control; ns: not significant. sh1: shSNX10-1; sh2: shSNX10-2; GAPDH: glyceraldehyde-3-phosphate dehydrogenase; LAMP-2A: lysosome-associated membrane protein type 2A; HSC70: heat shock cognate protein 70.

Lysosomes play a pivotal role in metabolic balance [14]. Our earlier work showed SNX10 governs glucose utilization in human IECs [17]. Yet, its influence on lysosomal performance warrants deeper exploration. Impaired lysosomal activity leads to buildup of undegraded material in the lumen and a compensatory rise in lysosomal numbers [24]. Immunofluorescence was employed to examine lysosomes in FHC and NCM460 cells ± SNX10, revealing greater lysosomal abundance in shSNX10 cells marked by LAMP-2A **(Figure 3b)**.

Lysosomes require a low internal pH to enable optimal function of their hydrolytic enzymes, critical for substrate breakdown. Given SNX10's established role in endosomal/lysosomal trafficking [5, 6] and its known association with V-ATPase [25], we investigated whether heightened DEPDC5 turnover in shSNX10 IECs resulted from exaggerated acidification of endosomal/lysosomal compartments. To test this, lysosomal content was assessed using Lyso-Tracker Red, a cell-permeable red-fluorescent dye that selectively accumulates in acidic organelles, providing specific visualization of functional lysosomes. Consistent with our prediction, SNX10 depletion markedly elevated lysosomal mass in both FHC and NCM460 cells **(Figure 3c)**. This observation was corroborated by flow cytometry, which detected greater uptake of the dye **(Figure 3d)**. Staining intensity further increased in both shNC and shSNX10 cells upon EBSS exposure. Subsequent application of CQ to block endosomal/lysosomal acidification reduced Lyso-Tracker Red signal in both groups; nevertheless, shSNX10 cells retained higher lysosomal staining than shNC cells even when co-treated with EBSS and CQ **(Figures 3c and 3d)**. Additionally, flow cytometry revealed that overexpressing DEPDC5 diminished lysosomal mass in shSNX10 IECs. Collectively, these data establish that SNX10 loss stimulates lysosome biogenesis, elevates lysosomal numbers and functionality in FHC and NCM460 cells, thereby augmenting hydrolytic capacity and accelerating CMA-dependent DEPDC5 breakdown via the lysosomal route. In summary, our evidence indicates that SNX10 depletion drives lysosome biogenesis and boosts lysosomal quantity and performance in FHC and NCM460 cells, favoring enhanced activity of lysosomal hydrolases and thus facilitating CMA-orchestrated DEPDC5 degradation through lysosomal mechanisms.

Depletion of SNX10 enhanced lysosomal membrane recruitment of mTORC1 and stimulated mTORC1 signaling

Lysosomes serve as key platforms for mTORC1 activation [15]. Recruitment of mTORC1 to the lysosomal membrane triggers its activation, whereas dissociation suppresses activity. We therefore assessed the impact of SNX10 loss on mTORC1 lysosomal positioning and observed substantially greater overlap between lysosome-associated membrane protein 2 (LAMP2) (red) and mTOR (yellow) in shSNX10 IECs **(Figure 4a)**, indicating that SNX10 knockdown promotes mTORC1 accumulation on lysosomal surfaces and thereby activates mTORC1 signaling.

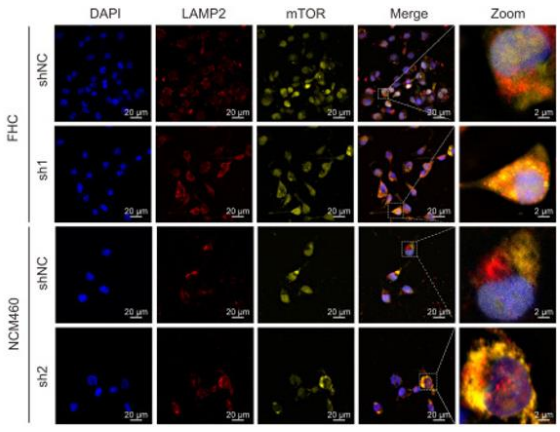

a)

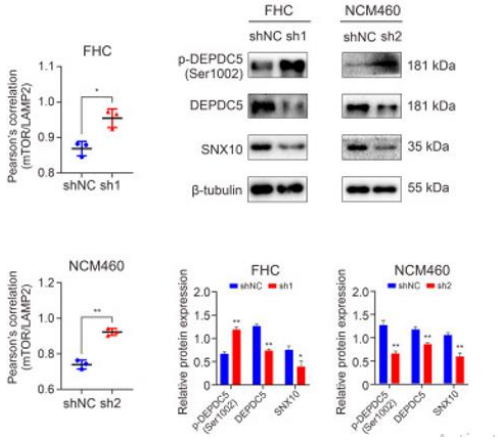

b)

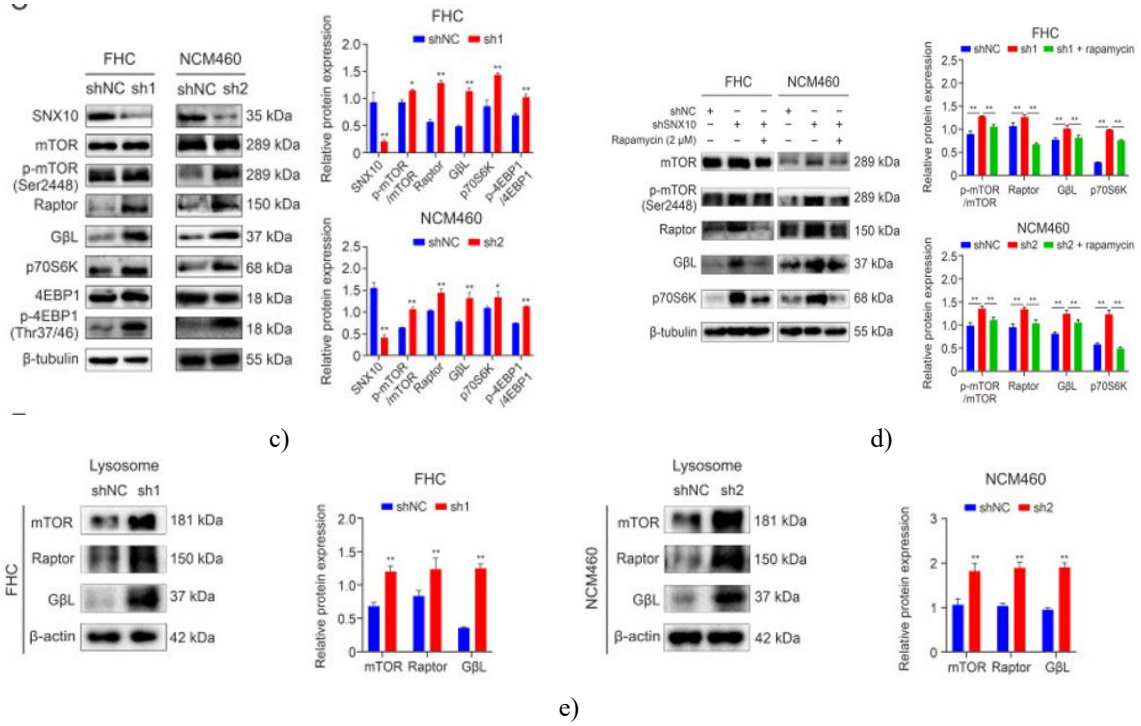

Figure 4. Loss of sorting nexin 10 (SNX10) facilitated lysosomal membrane association of mammalian target of rapamycin complex 1 (mTORC1), leading to pathway activation. (a) Confocal imaging of mammalian target of rapamycin (mTOR) (yellow) and lysosome-associated membrane protein 2 (LAMP2) (red) co-localization in shNC and shSNX10 IECs, with Pearson's correlation quantified via ImageJ. (b) Western blot assessment of phosphorylation status of DEP domain containing 5 (DEPDC5) in IECs following SNX10 depletion. (c) Protein levels of mTORC1 pathway components in shNC and shSNX10 IECs. (d) Western blot detection of mTORC1-related proteins post-rapamycin exposure. (e) Lysosomal fractionation followed by immunoblotting to evaluate mTORC1 lysosomal recruitment in FHC and NCM460 lines ± SNX10 knockdown. Values are means ± SD. ∗P < 0.05, ∗∗P < 0.01 versus control. sh1: shSNX10-1; sh2: shSNX10-2; Raptor: regulatory-associated protein of mTOR; GβL: G protein β-subunit-like protein.

DEPDC5 functions as an upstream suppressor of mTORC1. Prior reports indicate that phosphorylation at Ser1002 and Ser1530 by AKT1 and PIM1 impairs DEPDC5 function, relieving mTORC1 restraint [26]. We detected elevated DEPDC5 phosphorylation specifically at Ser1002 in SNX10-depleted cells **(Figure 4b)**, providing additional evidence for mTORC1 pathway stimulation in normal human IECs upon SNX10 loss. The core mTORC1 complex comprises mTOR, G protein β-subunit-like protein (GβL), and regulatory-associated protein of mTOR (Raptor). As anticipated, ratios of p-mTOR/mTOR (at Ser2448), p-4EBP1/4EBP1 (at Thr37/46), along with protein levels of Raptor, GβL, and p70S6K were all upregulated **(Figure 4c)**. Treatment with 2 μM rapamycin, a selective mTORC1 inhibitor, effectively suppressed this hyperactivation in shSNX10 IECs **(Figure 4d)**, confirming pathway engagement following SNX10 depletion. Moreover, restoring SNX10 expression normalized the aberrantly elevated mTORC1 activity in knockdown lines.

To substantiate these findings, lysosomes were purified, total lysosomal proteins extracted, and levels of mTORC1 subunits (mTOR, GβL, Raptor) evaluated by immunoblotting. Markedly higher abundance of these components was observed in lysosomal fractions from shSNX10 compared to shNC cells **(Figure 4e)**, indicating substantial mTORC1 clustering on lysosomal membranes and robustly supporting mTORC1 activation in SNX10-deficient IECs.

As the primary cellular energy-sensing cascade, mTORC1 signaling governs energy homeostasis, proliferation, protein synthesis, and autophagy, among others [15]. Heightened mTORC1 activity in SNX10-knockdown lines correlated with increased proliferation rates. Rescue experiments showed that SNX10 re-expression decelerated growth, impaired colony-forming capacity, while rapamycin mitigated the proliferation surge in shSNX10 cells. These results establish that the enhanced proliferative phenotype in SNX10-depleted IECs stems directly from intracellular mTORC1 pathway activation.

α-hederin suppressed the enhancement of lysosomal performance and CMA induction triggered by SNX10 depletion

SNX10 participates in controlling the endosomal/lysosomal trafficking essential for CMA [5, 6]. No prior investigations have explored whether α-hederin modulates lysosomal processes or influences CMA flux. To probe α-hederin's impact on lysosomes, we first identified suitable dosing **(Figure 5a)** and then monitored lysosomal alterations in α-hederin-exposed shSNX10 cells. Lyso-Tracker Red labeling revealed a substantial drop in average fluorescence intensity following α-hederin exposure in shSNX10 cells, signifying reduced lysosomal acidification **(Figure 5b)**, a finding validated by flow cytometry **(Figure 5c)**. As detailed in **Figures 2 and 3**, SNX10 loss expedited CMA-dependent DEPDC5 turnover via lysosomal mechanisms. We next assessed α-hederin's influence on CMA stimulation in shSNX10 cells. α-hederin exposure progressively elevated GAPDH levels while reducing SNX10, LAMP-2A, and HSC70 abundance, concurrently blocking DEPDC5 protein loss **(Figure 5d)**. Immunofluorescence confirmed that the aberrant rise in HSC70 seen in SNX10-depleted cells was reversed by α-hederin **(Figure 5e)**. Collectively, these observations offer initial proof that α-hederin curbs heightened lysosomal activity by boosting SNX10 levels, thereby dampening CMA flux and halting DEPDC5 breakdown in shSNX10 cells. For robust confirmation, total proteins were isolated from shNC and shSNX10 cells under basal conditions, EBSS stimulation, and/or medium-dose α-hederin, then probed for LAMP-2A, HSC70, and GAPDH **(Figure 5f)**. Outcomes demonstrated aberrant CMA hyperactivation post-SNX10 depletion, further amplified by EBSS, but mitigated by α-hederin. These patterns establish that α-hederin counteracts the augmented lysosome formation and elevated CMA flux induced by SNX10 loss.

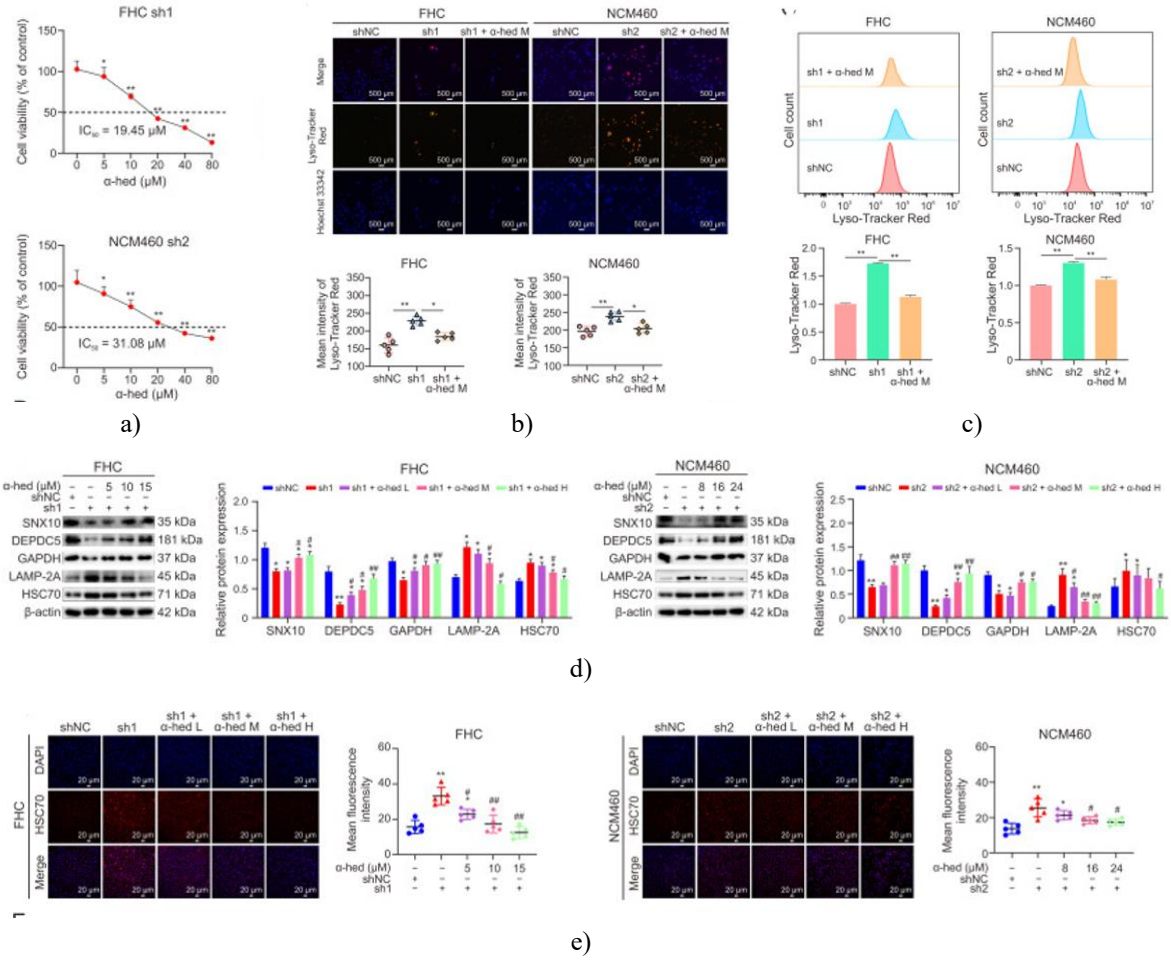

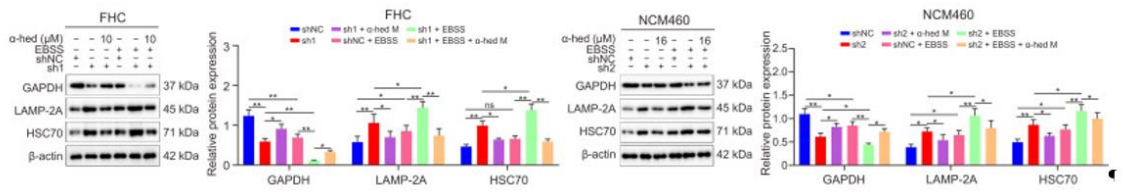

f)

Figure 5. α-hederin (α-hed) blocked sorting nexin 10 (SNX10)-driven lysosomal turnover of DEP domain containing 5 (DEPDC5) by suppressing chaperone-mediated autophagy (CMA) flux. (a) Viability of FHC shSNX10-1 (sh1) and NCM460 shSNX10-2 (sh2) cells assessed via 3-(4, 5-dimethylthiazol-2-yl)-2, 5 diphenyl tetrazolium bromide (MTT) assay after 24 h exposure to 0, 5, 10, 20, 40, and 80 μM α-hed. Half-maximal inhibitory concentration (IC50) values calculated and indicated. (b, c) α-hed effects on lysosomal performance evaluated by immunofluorescence (b) and flow cytometry (c). (d, e) Influence of α-hed on CMA flux in shSNX10 cells measured by Western blotting (d) and immunofluorescence (e). (f) CMA status in shNC and shSNX10 cells ± Earle's balanced salt solution (EBSS) and/or α-hed assessed via immunoblotting. Values shown as means ± SD. ∗P < 0.05, ∗∗P < 0.01 versus control, #P < 0.05, ##P < 0.01 versus shSNX10. α-hed L: low-dose α-hederin; α-hed M: medium-dose α-hederin; α-hed H: high-dose α-hederin; GAPDH: glyceraldehyde-3-phosphate dehydrogenase; LAMP-2A: lysosome-associated membrane protein type 2A; HSC70: heat shock cognate protein 70.

α-hederin, serving as a direct binder of SNX10 and DEPDC5, suppressed mTORC1 signaling by blocking CMA-dependent DEPDC5 turnover

As an upstream inhibitor of mTORC1, DEPDC5's involvement and mechanisms in oncogenesis, particularly colorectal cancer (CRC), remain underexplored. Given our discovery of physical SNX10–DEPDC5 association, we analyzed their protein correlation in colon adenocarcinoma (COAD; n=457) using the TIMER database, revealing a positive relationship **(Figure 6a)**. We further quantified SNX10 and DEPDC5 in normal human IECs versus CRC lines via qPCR and immunoblotting, detecting reduced abundance of both in malignant cells relative to normal counterparts **(Figures 6b and 6c)**. This aligns with earlier findings of diminished SNX10 in CRC patient tumors versus adjacent tissue [3] and lower DEPDC5 in CRC specimens [19]. A Pearson's plot yielded an R value of 0.7670 **(Figure 6d)**, confirming robust positive correlation. Thus, SNX10 not only physically interacts with DEPDC5 **(Figures 2e, 2f, 2g and 1j)** but also exhibits coordinated expression.

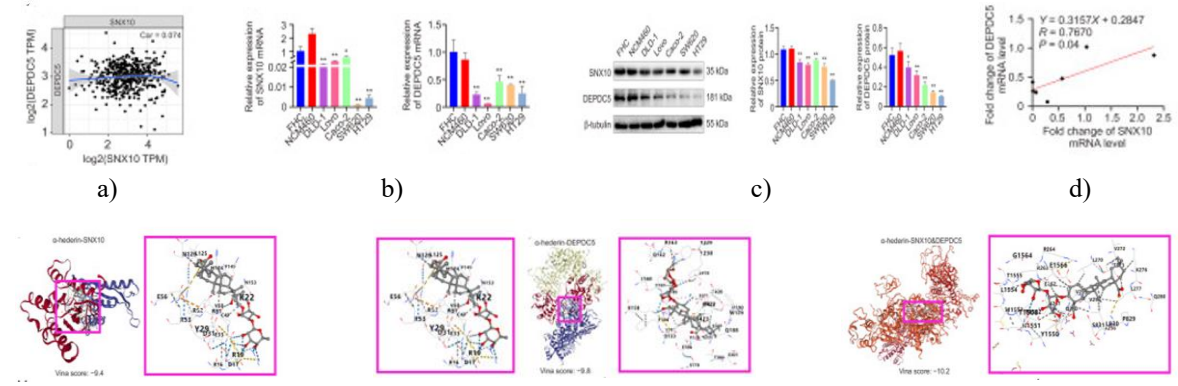

a) b) c) d)

e) f) g)

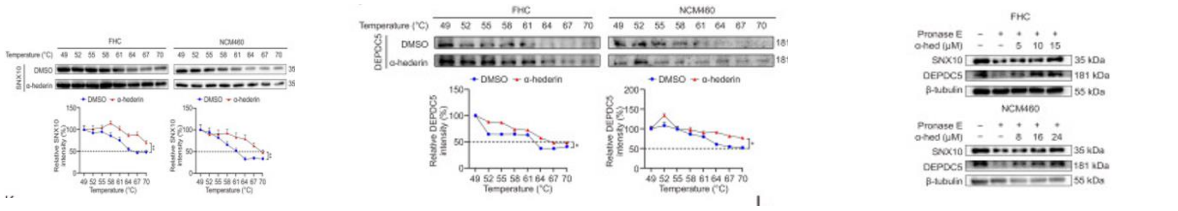

h) i) j)

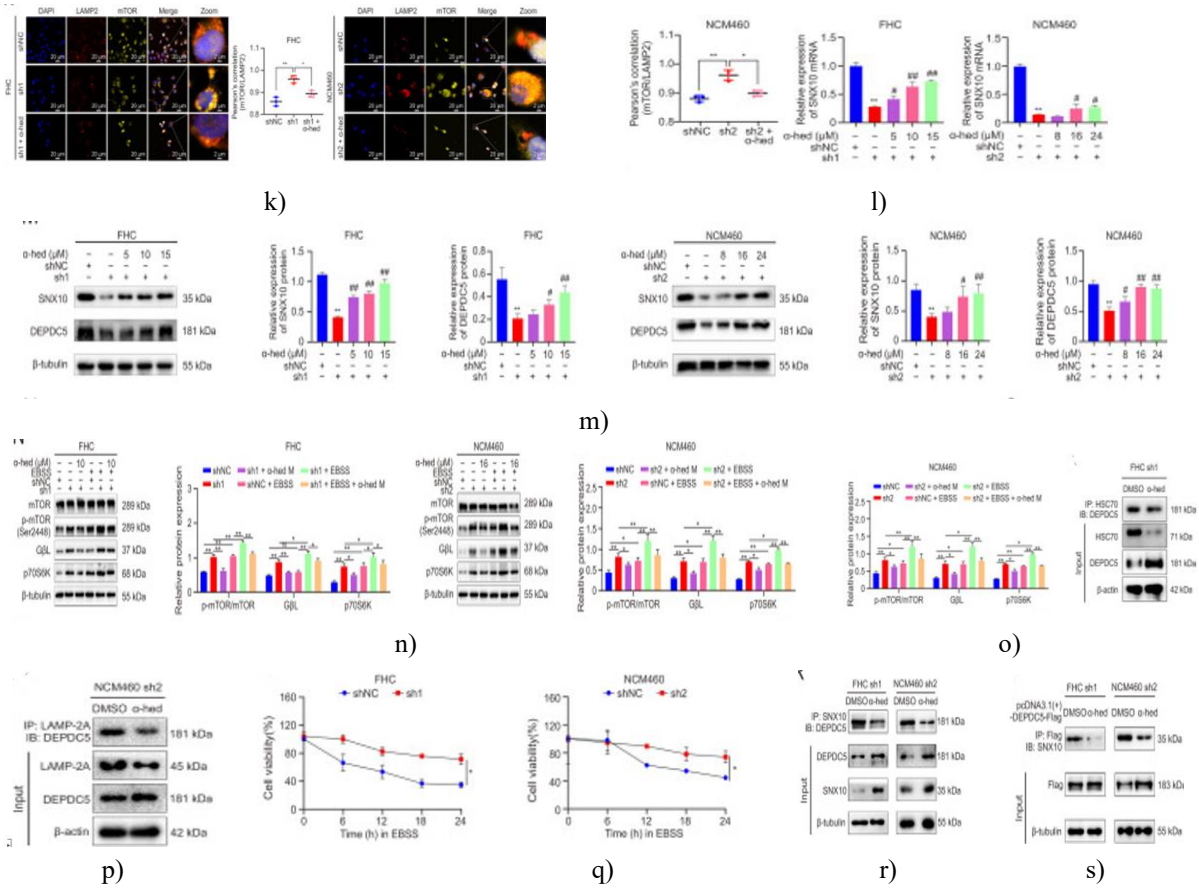

Figure 6. α-hederin (α-hed) restrained mammalian target of rapamycin complex 1 (mTORC1) signaling by preventing chaperone-mediated autophagy (CMA)-driven degradation of DEP domain containing 5 (DEPDC5). (a) Protein correlation between sorting nexin 10 (SNX10) and DEPDC5 evaluated via TIMER database. (b, c) SNX10 gene and protein levels in normal human intestinal epithelial cells (IECs) and colorectal cancer (CRC) lines determined by quantitative real-time polymerase chain reaction (qPCR) (B) and Western blotting (c). (d) Pearson's correlation analysis of SNX10 and DEPDC5. (E, F) 3D and 2D molecular docking of α-hed with SNX10 (e) and DEPDC5 (f). (g) 3D and 2D docking of α-hed with the SNX10–DEPDC5 complex. (h, i) Cellular thermal shift assay (CETSA) evaluation of SNX10 (h) and DEPDC5 (i) thermal stability. (j) Drug affinity responsive target stability (DARTS) confirmation of α-hed binding to SNX10 and DEPDC5. (k) Confocal assessment of mammalian target of rapamycin (mTOR) (yellow) and lysosome-associated membrane protein 2 (LAMP2) (red) overlap in FHC shSNX10-1 (sh1) and NCM460 shSNX10-2 (sh2) cells ± α-hed, with Pearson's correlation via ImageJ. (l) α-hed impact on SNX10 mRNA. (m) α-hed effects on SNX10 and DEPDC5 protein abundance. (n) mTORC1 status in shNC and shSNX10 cells ± Earle's balanced salt solution (EBSS) and/or α-hed via immunoblotting. (o, p) Co-immunoprecipitation (Co-IP) detection of DEPDC5 associations with heat shock cognate protein 70 (HSC70) (O) and lysosome-associated membrane protein type 2A (LAMP-2A) (P) in α-hed-treated shSNX10 cells, analyzed by Western blotting. (q) Viability via MTT assay over time for shNC and shSNX10 cells in EBSS. (r, s) Co-IP evaluation of SNX10–DEPDC5 interaction ± α-hed in FHC sh1 and NCM460 sh2 cells using anti-SNX10 (r) and anti-Flag (s) antibodies, with input/immunoprecipitate levels assessed by immunoblotting. Values are means ± SD. ∗P < 0.05, ∗∗P < 0.01 versus control, #P < 0.05, ##P < 0.01 versus shSNX10. DMSO: dimethyl sulfoxide; mTOR: mammalian target of rapamycin; GβL: G protein β-subunit-like protein; p70S6K: p70 ribosomal S6 kinase.

Since α-hederin elevated SNX10 abundance alongside DEPDC5 stabilization (by blocking its turnover) **(Figure 5d)**, we conducted in silico docking to explore binding modes. Interactions of α-hederin (PubChem CID: 73296) with SNX10 (PDB ID: 4PZG) or DEPDC5 (PDB ID: 6CET) were simulated, designating proteins as receptors and α-hederin as ligand **(Figures 6e and 6f)**. Docking yielded Vina scores of −9.4 for SNX10 and −9.8 for

DEPDC5, signifying robust affinity. Given prior evidence of SNX10–DEPDC5 association **(Figure 2)** and their positive expression correlation **(Figures 6a and 6d)**, we extended docking to the SNX10–DEPDC5 complex (protein–protein pose predicted via ZDOCK server), obtaining a Vina score of −10.2 **(Figure 6g)**. To confirm direct binding experimentally, cellular thermal shift assay (CETSA) and drug affinity responsive target stability (DARTS) were performed. CETSA demonstrated that α-hederin markedly improved thermal stability of both SNX10 **(Figure 6h)** and DEPDC5 **(Figure 6i)** versus DMSO control. DARTS similarly revealed protection of both proteins from Pronase E digestion by α-hederin **(Figure 6j)**. These results establish direct physical engagement of α-hederin with SNX10 and DEPDC5.

As established in **Figure 4**, SNX10 depletion drove mTORC1 recruitment to lysosomal membranes and pathway stimulation. α-hederin exposure substantially diminished overlap between LAMP2 (red) and mTOR (yellow) **(Figure 6k)** while increasing SNX10 mRNA **(Figure 6l)** and protein levels **(Figure 6m)**. To link mTORC1 hyperactivation in shSNX10 cells to CMA flux, proteins were harvested from shNC and shSNX10 lines ± EBSS and/or medium-dose α-hederin, then probed for mTOR, p-mTOR, GβL, and p70S6K. EBSS further amplified mTORC1 signaling in knockdown cells, whereas α-hederin countered this elevation **(Figure 6n)**. Co-IP further showed weakened DEPDC5 binding to HSC70 and LAMP-2A post-α-hederin in shSNX10 cells **(Figures 6o and 6p)**, indicating that mTORC1 upregulation from SNX10 loss requires CMA engagement and is reversible by α-hederin via SNX10 restoration. Heightened mTORC1 activity in knockdown lines promoted rapid proliferation. Even under EBSS-induced starvation, shSNX10 cells outgrew shNC counterparts, implying enhanced survival in nutrient scarcity **(Figure 6q)**. Given DEPDC5 turnover in shSNX10 cells and its mTORC1-suppressive role, we overexpressed DEPDC5 in knockdown lines and assessed growth via CCK8, colony formation, and EdU labeling. Overexpression curtailed the proliferation surge, consistent with DEPDC5 as an interacting partner **(Figures 2e, 2f, and 2j)** and co-expressed protein **(Figures. 6a and 6d)** of SNX10.

Synthesizing our data, we posited a ternary complex involving α-hederin, SNX10, and DEPDC5. Co-IP testing this revealed that α-hederin disrupted SNX10–DEPDC5 association **(Figures. 6r and 6s)**, thereby preserving DEPDC5 from CMA degradation **(Figure 6m)**, reducing mTORC1 lysosomal docking **(Figure 6k)**, and ultimately blunting mTORC1 activation in shSNX10 IECs **(Figure 6n)**.

α-hederin normalized heightened glycolysis in SNX10-depleted IECs

mTORC1 influences glucose and amino acid metabolism downstream via transcription factors like MYC proto-oncogene (c-Myc), often overexpressed in cancers [27, 28]. Glycolytic targeting represents a promising therapeutic avenue [29]. Key enzymes include lactate dehydrogenase A (LDHA) and pyruvate kinase M2 (PKM2) [30]. LDHA is c-Myc-regulated; its upregulation in tumors drives progression [31]. c-Myc also engages PKM2 to control the terminal glycolytic step and boosts expression of GLUT-1, LDHA, and hexokinase genes [32]. Elevated PKM2 enhances glucose consumption and lactate output, supporting tumor growth [33].

In shSNX10 lines, c-Myc levels rose, accompanied by increased LDHA and PKM2 **(Figures 7a and 7b)**. SNX10 restoration lowered protein abundance of these factors and reduced or normalized their mRNA relative to vector control. Enzymatic assays confirmed heightened lactate dehydrogenase (LDH) and pyruvate kinase (PK) activities in shSNX10 IECs **(Figure 7c)**, which declined upon SNX10 re-expression and was corroborated by immunofluorescence, affirming suppression of c-Myc-driven glycolytic effectors. α-hederin exposure diminished the intensified LDHA and PKM2 signals in shSNX10 cells, aligning with activity measurements showing elevated LDH and PK in knockdowns that reverted toward shNC levels dose-dependently with α-hederin **(Figure 7f)**. qPCR and immunoblotting across α-hederin doses similarly revealed reversal of upregulated c-Myc, LDHA, and PKM2 mRNA and protein in shSNX10 cells, approaching control levels **(Figures 7g and 7h)**. Thus, α-hederin counteracted the aberrant elevation of pivotal glycolytic enzymes LDH and PK in SNX10-deficient IECs.

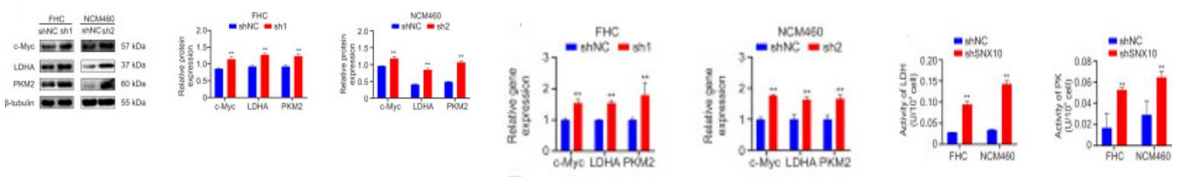

a) b) c)

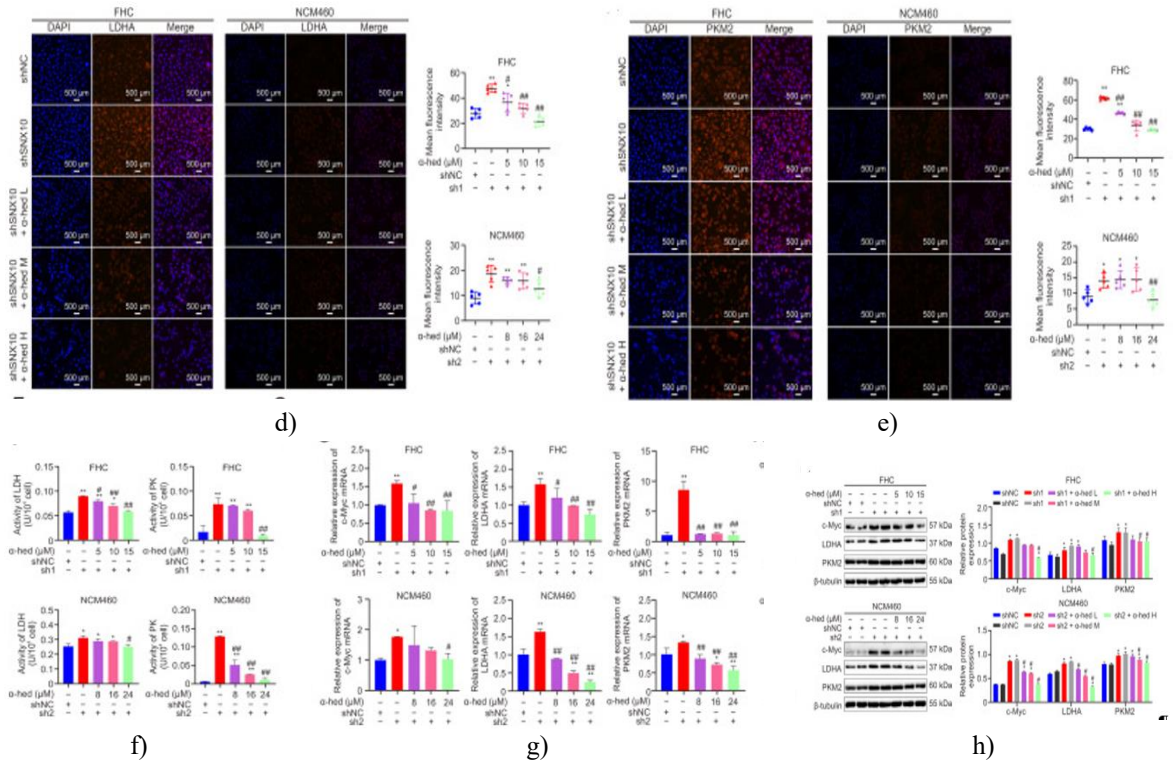

Figure 7. Influence of α-hederin (α-hed) on glycolytic activity in sorting nexin 10 (SNX10)-depleted cell lines. (a, b) Levels of glycolytic regulators, including MYC proto-oncogene (c-Myc), lactate dehydrogenase A (LDHA), and pyruvate kinase M2 (PKM2), were assessed by Western blotting (A) and quantitative real-time polymerase chain reaction (qPCR) (b). (c) Activities of lactate dehydrogenase (LDH) and pyruvate kinase (PK) were quantified using commercial kits in shNC and shSNX10 cells. (d, e) Effects of α-hed on LDHA (d) and PKM2 (e) abundance in shSNX10 cells evaluated via immunofluorescence. (f) Impact of α-hed on enzymatic function in shSNX10 cells. (g, h) α-hed modulation of c-Myc, LDHA, and PKM2 expression in shSNX10 cells measured by qPCR (g) and Western blotting (h). Values are means ± SD. ∗P < 0.05, ∗∗P < 0.01 versus shNC, #P < 0.05, ##P < 0.01 versus shSNX10. α-hed L: low-dose α-hederin; α-hed M: medium-dose α-hederin; α-hed H: high-dose α-hederin. sh1: shSNX10-1; sh2: shSNX10-2.

Colorectal cancer (CRC) currently represents a major public health challenge, severely impacting population well-being [1]. It typically arises from cumulative alterations in normal intestinal epithelial cells (IECs) triggered by diverse stressors, including metabolic imbalances [34], persistent inflammation [35], microbial imbalance [36], dysregulated immunity [37], and hereditary predispositions or acquired mutations [38] that inactivate suppressors or activate oncogenes. To endure such hostile conditions, normal IECs adapt through altered proliferation, autophagy, and metabolism. Prolonged exposure to these insults can drive genetic instability, culminating in neoplastic transformation.

SNX10 acts as a suppressor in CRC [3, 4] and critically modulates chaperone-mediated autophagy (CMA) flux [3, 9, 10], a process markedly elevated in CRC lines [4, 13]. CMA selectively degrades proteins bearing KFERQ-like motifs via chaperone-assisted lysosomal delivery [14], with lysosomes functioning as central metabolic nodes that control pathways like mTORC1 [15]. Our earlier work revealed that SNX10 depletion in normal human IECs abnormally boosted proliferation and glucose utilization, reduced DEPDC5 protein, and showed reversal by α-hederin. This implied potential SNX10 control over DEPDC5—a suppressor in gastrointestinal tumors [18]—possibly linked to IEC malignant progression. The precise regulatory mechanism and α-hederin's involvement remained unclear, prompting us to explore early CRC drivers. Here, we established that SNX10 loss lowers DEPDC5 protein via post-transcriptional means and lysosomal routing **(Figure 1)**. DEPDC5 harbors two conserved CMA motifs (QKVEF and VRLEQ) across species **(Figure 2a)**, qualifying it as a novel CMA target confirmed by Co-IP **(Figures 2h and 2i)**, lysosomal fractionation **(Figure 2k)**, and confocal analysis **(Figure 2l)**. We newly identified DEPDC5 as an SNX10 partner **(Figures 2e, 2f, 2g, and 2j)**, with SNX10 governing CMA by direct binding and lysosomal shuttling of DEPDC5 **(Figures 2 and 3)**. We also first demonstrated positive

SNX10–DEPDC5 expression correlation **(Figures 6a and 6d)**. Together, these reveal a previously unknown post-translational control of DEPDC5 by SNX10.

Lysosomes serve as key platforms for mTORC1 signaling [14, 15]. Our prior data linked SNX10 to IEC glucose handling [17], but lysosomal regulation needed clarification. Presently, we showed SNX10 depletion augments lysosomal performance and CMA flux, driving DEPDC5 CMA turnover **(Figure 3)**. As an upstream mTORC1 inhibitor [39], reduced DEPDC5 from SNX10 loss promoted mTORC1 lysosomal membrane association **(Figures 4a and 4e)** and pathway stimulation **(Figure 4c)**, validated by rapamycin blockade **(Figure 4d)**.

Enhanced CMA has been tied to elevated glycolysis supporting rapid growth in lung [40], breast [12], and colorectal cancers [13]. We observed heightened glycolysis in SNX10-depleted cells via increased LDH and PK activity **(Figures 7a-7c)**. SNX10 restoration mitigated DEPDC5 loss, mTORC1 activation, and glycolytic surge, confirming SNX10's roles and CMA–glycolysis interplay in normal IECs.

α-hederin's actions on lysosomal turnover and CMA remain largely unstudied. We demonstrated α-hederin curbs heightened lysosomal activity and blocks CMA-driven DEPDC5 breakdown in SNX10-deficient cells **(Figure 5)**, consequently suppressing mTORC1 **(Figure 6)**. Building on established SNX10–DEPDC5 binding **(Figure 2)** and correlation **(Figures 6a and 6d)**, we newly proved direct α-hederin engagement with both proteins **(Figures 6h-6j)**. Further, we uncovered ternary interplay: α-hederin disrupts SNX10–DEPDC5 association **(Figures 6r and 6s)**, preserving DEPDC5 **(Figure 6m)**. This, alongside weakened DEPDC5 links to HSC70 and LAMP-2A post-α-hederin **(Figures 6o and 6p)**, halts CMA-mediated loss, reduces mTORC1 lysosomal recruitment **(Figure 6k)**, and dampens pathway activity **(Figure 6n)**. Resultantly, α-hederin counters accelerated growth, enhances nutrient-stress resilience **(Figure 6q)**, and normalizes glycolysis **(Figure 7)** in shSNX10 IECs by elevating SNX10 and stabilizing DEPDC5. Overall, α-hederin impedes CMA-dependent DEPDC5 turnover through SNX10 upregulation and complex disruption, thereby restraining mTORC1/c-Myc signaling and downstream glycolysis, ultimately hindering IEC oncogenic conversion **(Figure 8)**.

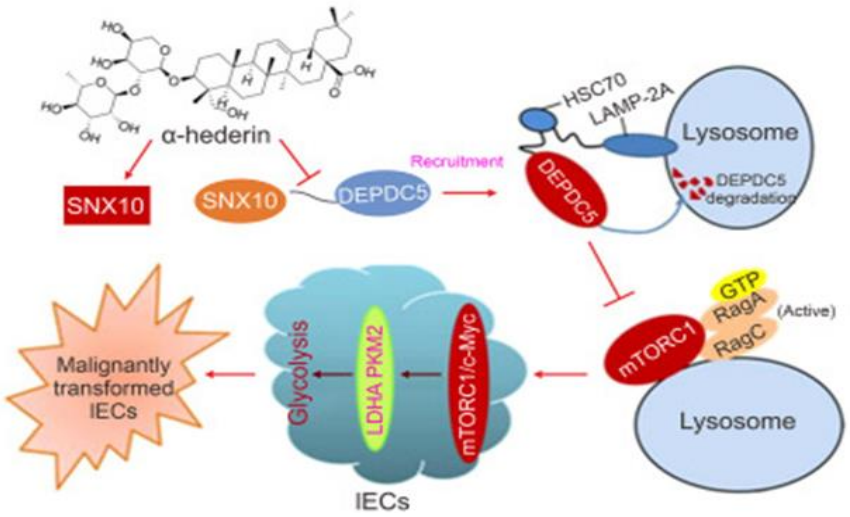

Figure 8. Schematic illustrating the mechanism by which α-hederin normalizes glycolytic flux and blocks oncogenic progression in normal human intestinal epithelial cells (IECs). SNX10: sorting nexin 10; DEPDC5: DEP domain containing 5; HSC70: heat shock cognate protein 70; LAMP-2A: lysosome-associated membrane protein type 2A; mTORC1: mammalian target of rapamycin complex 1; IECs: intestinal epithelial cells; c-Myc: MYC proto-oncogene; LDHA: lactate dehydrogenase A; PKM2: pyruvate kinase M2.

Our investigations newly establish SNX10 as a critical modulator of DEPDC5, demonstrating both positive expression correlation and robust physical association. We further uncover an undisclosed function of SNX10 in facilitating CMA-dependent DEPDC5 turnover, along with the interplay linking CMA to glycolysis and potentially to IEC oncogenic conversion. These observations position SNX10 and DEPDC5 as attractive therapeutic candidates for CRC interception and management, while revealing substantial promise for α-hederin in countering IEC malignant progression through SNX10 elevation and consequent DEPDC5 stabilization.

Overall, this work offers fresh insights into α-hederin's protective effects against IEC oncogenic shift, underscoring the central contribution of SNX10-orchestrated CMA–glycolysis crosstalk to malignant evolution, the value of SNX10 in illuminating initial CRC triggers, and the importance of SNX10-driven CMA-mediated DEPDC5 breakdown as a novel process in CRC initiation and advancement.

Conclusion

We are the first to demonstrate that α-hederin suppresses CMA flux via upregulation of SNX10, thereby preventing lysosomal-mediated DEPDC5 loss, restraining mTORC1 activation, and subsequently modulating IEC glycolysis. These results carry important ramifications for strategies aimed at averting oncogenic transformation of normal human intestinal epithelial cells.

Acknowledgments: None

Conflict of Interest: None

Financial Support: None

Ethics Statement: None

References

1. F. Bray, M. Laversanne, H. Sung, et al., Global cancer statistics 2022: GLOBO-CAN estimates of incidence and mortality worldwide for 36 cancers in 185 countries, CA Cancer J. Clin. 74 (2024) 229e263.
2. M. Pinheiro, D.N. Moreira, M. Ghidini, Colon and rectal cancer: An emergent public health problem, World J. Gastroenterol. 30 (2024) 644e651.
3. S. Zhang, B. Hu, Y. You, et al., Sorting nexin 10 acts as a tumor suppressor in tumorigenesis and progression of colorectal cancer through regulating chaperone mediated autophagy degradation of p21(Cip1/WAF1) , Cancer Lett. 419 (2018) 116e127.
4. S. Zhang, Z. Yang, W. Bao, et al., SNX10 (sorting nexin 10) inhibits colorectal cancer initiation and progression by controlling autophagic degradation of SRC, Autophagy 16 (2020) 735e749.
5. B. Qin, M. He, X. Chen, et al., Sorting nexin 10 induces giant vacuoles in mammalian cells, J. Biol. Chem. 281 (2006) 36891e36896.
6. L. Ye, L.R. Morse, R.A. Battaglino, Snx10: A newly identified locus associated with human osteopetrosis, IBMS Bonekey 2013 (2013), 421.
7. Q. Yang, R. Wang, L. Zhu, Chaperone-mediated autophagy, Adv. Exp. Med. Biol. 1206 (2019) 435e452.
8. J. Rios, A. Sequeida, A. Albornoz, et al., Chaperone mediated autophagy sub-strates and components in cancer, Front. Oncol. 10 (2021), 614677.
9. Y. You, W. Li, S. Zhang, et al., SNX10 mediates alcohol-induced liver injury and steatosis by regulating the activation of chaperone-mediated autophagy, J. Hepatol. 69 (2018) 129e141.
10. W. Lee, H.Y. Kim, Y.J. Choi, et al., SNX10-mediated degradation of LAMP-2A by NSAIDs inhibits chaperone-mediated autophagy and induces hepatic lipid accumulation, Theranostics 12 (2022) 2351e2369.
11. C. Chelakkot, V.S. Chelakkot, Y. Shin, et al., Modulating glycolysis to improve cancer therapy, Int. J. Mol. Sci. 24 (2023), 2606.
12. R. Chen, P. Li, Y. Fu, et al., Chaperone-mediated autophagy promotes breast cancer angiogenesis via regulation of aerobic glycolysis, PLoS One 18 (2023), e0281577.
13. R. Chen, Y. Zhang, Y. Ge, et al., LAMP-2A overexpression in colorectal cancer promotes cell growth and glycolysis via chaperone-mediated autophagy, Oncol. Lett. 27 (2023), 33.
14. C. Settembre, R.M. Perera, Lysosomes as coordinators of cellular catabolism, metabolic signalling and organ physiology, Nat. Rev. Mol. Cell Biol. 25 (2024) 223e245.
15. C. Goul, R. Peruzzo, R. Zoncu, The molecular basis of nutrient sensing and signalling by mTORC1 in metabolism regulation and disease, Nat. Rev. Mol. Cell Biol. 24 (2023) 857e875.
16. B. Carroll, E.A. Dunlop, The lysosome: A crucial hub for AMPK and mTORC1 signalling, Biochem. J. 474 (2017) 1453e1466.

17. H. Feng, J. Tan, Q. Wang, et al., a-hederin regulates glucose metabolism in intestinal epithelial cells by increasing SNX10 expression, Phytomedicine 111 (2023), 154677.
18. Y. Pang, F. Xie, H. Cao, et al., Mutational inactivation of mTORC1 repressor gene DEPDC5 in human gastrointestinal stromal tumors, Proc. Natl. Acad. Sci. USA 116 (2019) 22746e22753.
19. S. Solanki, K. Sanchez, V. Ponnusamy, et al., Dysregulated amino acid sensing drives colorectal cancer growth and metabolic reprogramming leading to chemoresistance, Gastroenterology 164 (2023) 376e391.e13.
20. Y. Zhan, K. Wang, Q. Li, et al., The novel autophagy inhibitor alpha-hederin promoted paclitaxel cytotoxicity by increasing reactive oxygen species accumulation in non-small cell lung cancer cells, Int. J. Mol. Sci. 19 (2018), 3221.
21. C. Fang, Y. Liu, L. Chen, et al., a-Hederin inhibits the growth of lung cancer A549 cells in vitro and in vivo by decreasing SIRT6 dependent glycolysis, Pharm. Biol. 59 (2021) 11e20.
22. J. Sun, Y. Feng, Y. Wang, et al., a-hederin induces autophagic cell death in colorectal cancer cells through reactive oxygen species dependent AMPK/mTOR signaling pathway activation, Int. J. Oncol. 54 (2019) 1601e1612.
23. Q. Wang, H. Feng, Z. Li, et al., a-Hederin induces human colorectal cancer cells apoptosis through disturbing protein homeostasis, Chem. Biol. Interact. 386 (2023), 110785.
24. F.M. Platt, B. Boland, A.C. van der Spoel, The cell biology of disease: Lysosomal storage disorders: The cellular impact of lysosomal dysfunction, J. Cell Biol. 199 (2012) 723e734.
25. Y. Chen, B. Wu, L. Xu, et al., A SNX10/V-ATPase pathway regulates ciliogenesis in vitro and in vivo, Cell Res. 22 (2011) 333e345.
26. S.K.R. Padi, N. Singh, J.J. Bearss, et al., Phosphorylation of DEPDC5, a component of the GATOR1 complex, releases inhibition of mTORC1 and promotes tumor growth, Proc. Natl. Acad. Sci. USA 116 (2019) 20505e20510.
27. M. Ala, Target c-Myc to treat pancreatic cancer, Cancer Biol. Ther. 23 (2022) 34e50.
28. W. Cai, W. Ni, Y. Jin, et al., TRIP13 promotes lung cancer cell growth and metastasis through AKT/mTORC1/c-Myc signaling, Cancer Biomark 30 (2021) 237e248.
29. D.R. Schmidt, R. Patel, D.G. Kirsch, et al., Metabolomics in cancer research and emerging applications in clinical oncology, CA Cancer J. Clin. 71 (2021) 333e358.
30. C. Wang, Y. Li, S. Yan, et al., Interactome analysis reveals that lncRNA HULC promotes aerobic glycolysis through LDHA and PKM2, Nat. Commun. 11 (2020), 3162.
31. W. Yang, Y. Wei, T. Wang, et al., Cytoplasmic localization of SETDB1-induced Warburg effect via c-MYC-LDHA axis enhances migration and invasion in breast carcinoma, Int. J. Mol. Med. 53 (2024), 40.
32. B. Wu, Z. Liang, H. Lan, et al., The role of PKM2 in cancer progression and its structural and biological basis, J. Physiol. Biochem. 80 (2024) 261e275.
33. K. Duan, K. Fang, C. Sui, TFAIP6 facilitates hepatocellular carcinoma cell glycolysis through upregulating c-myc/PKM2 axis, Heliyon 10 (2024), e30959.
34. S. Yan, J. Chang, X. Hao, et al., Berberine regulates short-chain fatty acid metabolism and alleviates the colitis-associated colorectal tumorigenesis through remodeling intestinal flora, Phytomedicine 102 (2022), 154217.
35. Y. Ji, T. Tao, J. Zhang, et al., Comparison of effects on colitis-associated tumorigenesis and gut microbiota in mice between Ophiocordyceps sinensis and Cordyceps militaris, Phytomedicine 90 (2021), 153653.
36. Y. Zhou, Y. Feng, R. Cen, et al., San-Wu-Huang-Qin decoction attenuates tumorigenesis and mucosal barrier impairment in the AOM/DSS model by targeting gut microbiome, Phytomedicine 98 (2022), 153966.
37. Y. Zhang, N. Chai, Z. Wei, et al., YYFZBJS inhibits colorectal tumorigenesis by enhancing Tregs-induced immunosuppression through HIF-1a mediated hypoxia in vivo and in vitro, Phytomedicine 98 (2022), 153917.
38. R. Yin, B. Song, J. Wang, et al., Genome-wide association and transcriptome-wide association studies identify novel susceptibility genes contributing to colorectal cancer, J. Immunol. Res. 2022 (2022), 5794055.
39. T. Ribierre, C. Deleuze, A. Bacq, et al., Second-hit mosaic mutation in mTORC1 repressor DEPDC5 causes focal cortical dysplasia-associated epilepsy, J. Clin. Investig. 128 (2018) 2452e2458.
40. M. Kon, R. Kiffin, H. Koga, et al., Chaperone-mediated autophagy is required for tumor growth, Sci. Transl. Med. 3 (2011), 109ra117.